Highly Charged Ion - Secondary Ion Mass Spectrometry (HCI-SIMS): Towards Metrology Solutions for Sub 100 nm Technology Nodes

T. Schenkel[1], A. Krämer, and K. N. Leung
E. O. Lawrence Berkeley National Laboratory, Berkeley, CA 94720

A. V. Hamza, J. W. McDonald, and D. H. Schneider
Lawrence Livermore National Laboratory, Livermore, CA 94550

The transition to semiconductor design nodes below 100 nm will create high demands on metrology solutions for the detection and chemical characterization of defects and particles throughout all processing steps. The compositional analysis of particles with sizes below about 20 nm is one particular challenge. We describe progress in the development of a highly charged ion based secondary ion mass spectrometry (HCI-SIMS) schemes aimed at addressing this challenge. Using ions like Xe^{48+} as projectiles increases secondary ion yields by several orders of magnitude and enables the application of coincidence counting techniques for the characterization of nano-environments of selected species. Additionally, an ion emission microscope was developed for defect imaging and we report examples of its application. We discuss steps of combining beam focusing, coincidence analysis and emission microscopy to enable compositional analysis of sub 20 nm size particles.

1. Introduction

The analysis of surfaces and semiconductor structures faces the problem of increasing demands on lateral resolution and detection sensitivity. According to the International Technology Roadmap for Semiconductors, the detection and chemical characterization of particles with diameters of less than 20 nm will become important for technology nodes below 100 nm, which are currently anticipated for 2005 [1]. It is interesting to note that the need for chemical analysis of these small particles coincides with a new analytical challenges in nanoscience were nanocrystals with comparable dimensions are investigated for their unique properties [2]. Scanning electron microscopy (SEM) in combination with EDX (energy dispersive x-ray spectroscopy) or AES (Auger electron spectroscopy) have advanced the field of defect and particle characterization to amazing levels of lateral resolution (few nm) with high (~0.1 %) detection sensitivities. Scanning probe techniques such as atomic force microscopy (AFM) are nondestructive and can deliver topographical information on an even smaller length scale, down to atomic resolution in special applications. However, AFM generally does not deliver information on the chemical composition of particles. The latter is crucial for the pinpointing of contamination sources [3].

Elemental composition and chemical structure of surfaces can be probed by static secondary ion mass spectrometry, most widely in time-of-flight mode (TOF-SIMS). TOF-SIMS allows the imaging of the top monolayers of surfaces with a few hundred nm resolution and can detect secondary ions over the full mass range (up to a few thousand amu) in parallel. The lateral resolution in adaptations of focused ion beam systems with SIMS allows imaging of the elemental composition of samples with 10 to 30 nm

[1] Email: T_Schenkel@LBL.gov

resolution [4-8]. Here, SIMS is typically operated in quadrupole mode, where selected secondary ion masses are scanned, and the analysis mode is in the dynamic regime. In dynamic SIMS the beam currents are sufficiently high to equilibrate sample and beam, and the erosion rate is high enough to allow for 3D analysis of samples. The flip side of this ability is the loss of surface sensitivity. Monolayers of material are consumed before sufficient information on the chemical composition of the top layers of a sample can be collected. Diebold et al. compared the capabilities of AES, SEM with EDX and TOF-SIMS for the characterization of sub-micron (100 and 300 nm diameters) particles (Al, TiO_2 and Al_2O_3) on one micron thick SiO_2 layers [9]. Important advantages of TOF-SIMS are the unlimited mass range and parallel detection of secondary ions that can deliver information on the chemical structure of particles from the detection of molecular ions, and also allows the identification of organic contaminants. A key advantage of electron based techniques over SIMS is their high lateral resolution of a few nm.

SIMS is inherently a destructive technique, since the signal -secondary ions-constitutes a small fraction of material that is transferred from the sample into the gas phase. At a particle density of 5E22 atoms/cm3, or 50 atoms/nm^3, a particle with a diameter of 20 nm contains about 2E5 atoms. The efficiency of signal generation in SIMS is described by the ionization probability, defined as the number of secondary ions that are generated per amount of sputtered material. Ionization probabilities are often ~0.1% or smaller, but can be increased to 10% and more in special cases by means of oxygen (for positive secondary ions) and cesium (for negative secondary ions) beams, or through the introduction of oxygen flood gas during analysis. Also, the move to polyatomic projectiles has long been suggested to increase ionization probabilities. Fuoco et al. recently quantified this yield enhancement in a study of sputtering and ion formation from poly(methylmetacylate) (PMMA) layers with SF_5^+ projectiles [10].

An ideal instrument for particle characterization would combine an SEM for imaging and particle localization with optimized secondary ion detection of an improved TOF-SIMS system. The ideal TOF-SIMS system would have a lateral resolution of 10 to 20 nm and form elemental and molecular secondary ions with high ionization probabilities. The use of highly charged projectiles, like Xe^{44+} or Au^{69+}, was fund to increase secondary ion yields from thin SiO_2 layers by three orders of magnitude [11]. Detection of several secondary ions following the impact of one projectile allows the application of coincidence counting techniques from which chemical structure information on a length scale of about 5 nm can be derived [12, 13]. Imaging of secondary electrons and secondary ions in an ion emission microscope with highly charged projectiles was demonstrated at the 800 nm level [14]. Highly charged ions can improve the amount of information that can be extracted from a nanometer size particle before the particle is eroded. In the following we describe the status of SIMS with highly charged ions (HCI-SIMS), and discuss the path to the development of a metrology tool capable of characterizing the chemical structure and elemental composition of <50 nm particles on silicon surfaces.

2. Interaction of highly charged ions with solids

Sputtering is the process in which atoms, molecules and clusters are emitted from (mostly) solid materials following the impact of energetic atoms or ions. Projectiles with kinetic energies from a few tens of eV to many MeV transfer momentum to target

electrons and nuclei in inelastic and elastic collisions. Secondary ions constitute generally a small (<1%) fraction of the sputtered material. When the goal is to maximize secondary ion yields, one promising strategy is to maximize the degree of electronic excitation of target material in the course of the impact of projectiles. In Tab. 1, we compare characteristic energy loss rates, or stopping powers, for a series of projectiles.

Projectile	**Mechanism of energy deposition**	**Effective Stopping Power**
KeV ion	elastic collisions (nuclear stopping)	few keV/nm
MeV/u heavy ion	inelastic collisions (electronic stopping)	tens of keV/nm
Slow Cluster Ion (e. g., $Au_{n=5}$, SF_5^+)	dense elastic collisions (thermal spike)	n × few keV/nm
Swift Cluster Ion (e. g., C_{60})	dense inelastic collisions (electronic stopping)	n × tens of keV/nm
Slow, highly charged ion (e. g., Au^{69+})	intense, ultrafast electronic excitation	100 keV/nm

Table 1: Comparison of energy deposition scales for different ion-solid interaction regimes.

In conventional SIMS, the degree of electronic excitation, or ionization of target atoms is small, but secondary ion yields can be enhanced by chemical means. In the latter a beam of cesium ions is used to reduce the work function of a target surface and aid the formation of negative ions, or an oxygen beam facilitates the localization of electrons in ionic bonds and thus aids the emission of positive secondary ions. We note that these chemical methods can also be employed while target ionization is maximized. Highly charged ions with keV energies deposit their potential energy (the sum of the binding energies of the electrons that were removed when forming the ion) within about 10 fs, close to the target surface [15]. This fast charge equilibration constitutes an energy deposition rate matched only by MeV/u heavy ions, or heavy clusters with MeV energies. Secondary ions and neutrals are emitted following the intense, ultrafast electronic excitation and ionization of the target by a highly charged ion. The ionization probabilities for positive secondary ions from heavy metal oxide samples were found to increase as a function of projectile charge state. This increased ionization probability enables analysis of trace impurities with increased sensitivity [16]. To date this is only an indication since the dynamic range of our HCI-SIMS system has limited the detection of impurities on silicon surfaces to about 0.1 % of a monolayer [21].

Positive secondary ion emission yields for a series of target materials are shown in Fig. 1 for Th^{70+} ions. The figure displays positive secondary ions detected per incident ion. Yields for thin SiO_2 layers on silicon exceed one, i. e., at average more than one secondary ion was detected following the impact of one projectile. As the resistivity of

target materials decreases, secondary ion yields decrease to values consistent with collisional sputtering. Oxides and oxidized surfaces are favorable for HCI-SIMS, clean metals are not.

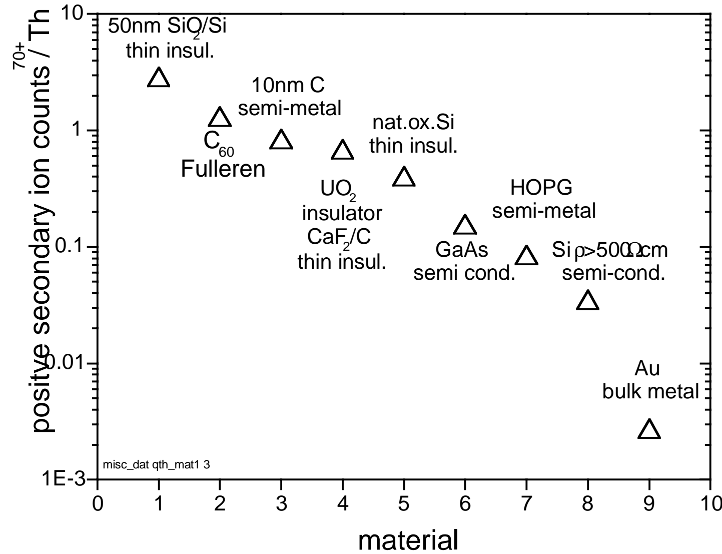

Figure 1.: Positive secondary ion counts detected per incident Th^{70+} ion (E_{kin}=280 keV) from a series of materials. The detection efficiency of the TOF spectrometer of ~0.15 was not included.

Many secondary ion emission phenomena observed for slow, highly charged ions (SHCI) had also been found for swift heavy ions [17], where electronic excitation is facilitated through high values of electronic energy loss, rather than fast charge equilibration. A key difference is that slow (<10 keV/u) HCI can be formed in a rather compact setup with a footprint of less than about 1 m^2 [18], and do not require the large (>10 m) accelerator structures that are needed to form fast (>100 keV/u) heavy ions.

3. Experimental

Highly charged ions (HCI) are produced in an Electron Beam Ion Trap [18] and extracted with kinetic energies of 3 to 25 kV times ion charge, q, i. e., $E_{kin}=U_{extr}\times q$ (keV). Beams of charge state selected ions reach a wafer after momentum analysis in a 90° bending magnet. Scanning the magnetic field yields the distribution of extracted ion charge states. In Fig. 2, we show an example of xenon ions extracted with U_{extr}=7 kV. The EBIT delivers beams of e. g. Xe^{44+} ions with an intensity of about 1E6 ions/s. For TOF-SIMS, a beam current of about 1000 ions/s is sufficient, since each TOF cycle is triggered by the impact of one single projectile. In negative polarity, secondary electrons and in positive polarity the emission of large numbers of protons is used as a start signal, [19-21]. Secondary ions are extracted into a reflectron type mass spectrometer. The mass resolution, m/dm, in single ion triggering is about 1000 at m=28 u. Focusing of an Ar^{18+} beam with ~1E6 ions/s into a 20 micron spot was reported by Marrs et al. [22]. In our first focusing efforts at the new EBIT facility in Berkeley we transported about 1E4 ions/s into a 5 micron spot.

TOF cycles of secondary ions emitted from individual projectiles are simply summed up to form a spectrum (histogram mode). Alternatively, TOF cycles can be stored individually, and can then be searched by coincidence analysis.

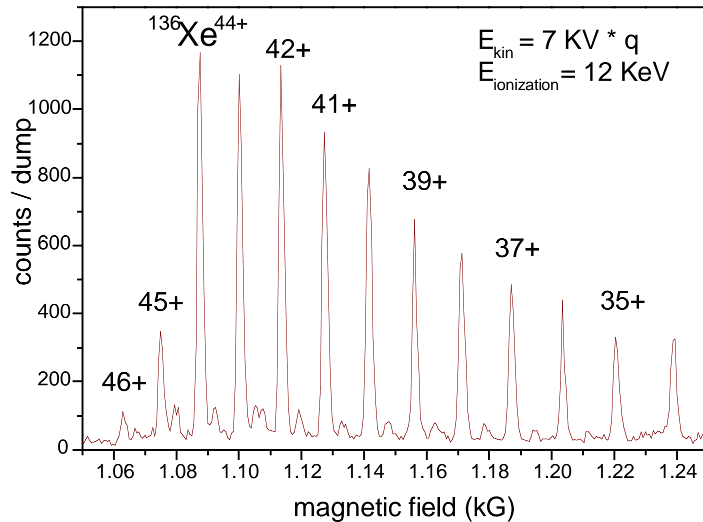

Figure 2.: Spectrum of Xe^{q+} ions extracted from EBIT with an extraction potential of 7 kV and analyzed with a 90° bending magnet.

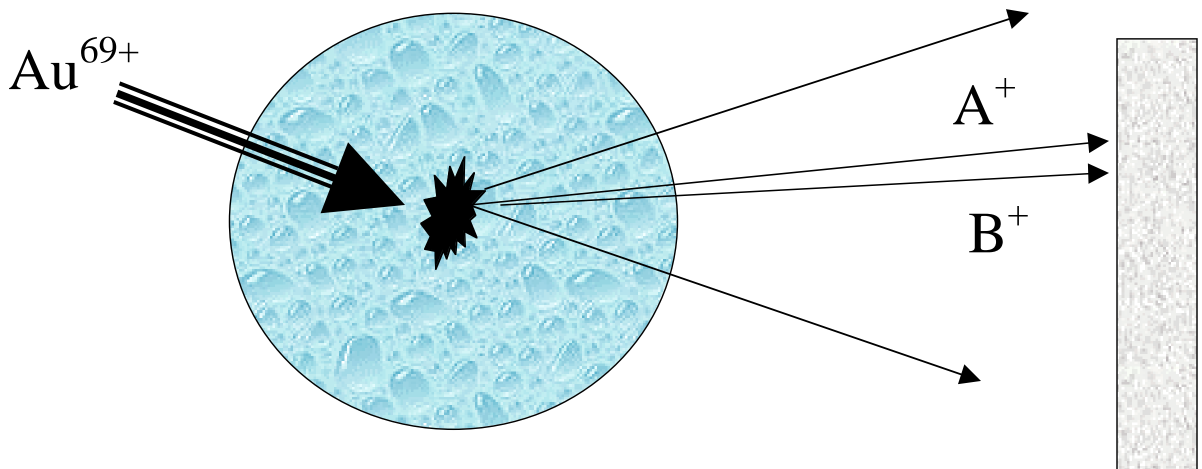

Figure 3: Schematic of the coincidence analysis experiment in TOF-SIMS with highly charged projectiles.

Figure 3 illustrates the principle of coincidence analysis (for more details see Ref 12 and 13). A single projectile impinges on a sample and emits several secondary ions, two of which are detected. The area of secondary ion emission is not known but it can be estimated to be about 10 nm in diameter from the size of defects induced by single ion

impacts [23, 24]. The detection of multiple secondary ions from one projectile impact delivers thus information on the chemical composition of a species (an elemental ion, molecular cluster) on the length scale of several nanometers. Coincidence analysis alone does not deliver imaging information. However, in combination with stigmatic imaging or rastering of a focused beam, it can extend the effective lateral resolution.

3. Results and Discussion

3.1. Analysis of cesiated Si clusters

We applied the coincidence analysis scheme to a sample of silicon nano-clusters. The clusters had been deposited onto a highly oriented pyrolitic graphite sample with sub-monolayer coverage. Figure 4 a) shows an atomic force microscopy image of the nano-cluster sample. The mean cluster diameter was about 200 nm. The silicon nano-clusters where enriched with cesium. We collected HCI-SIMS data in list mode and used the cesium to test the correlation between silicon and cesium secondary ions. Figure 4 b) shows a section of a TOF spectrum. The emission of silicon and cesium ions is strongly correlated, with a correlation coefficient, $C(Cs^+, Si^+)=6.5$. On the contrary, the emission of cesium and carbon ions is not correlated. This examples demonstrates the principle of coincidence analysis of small particles.

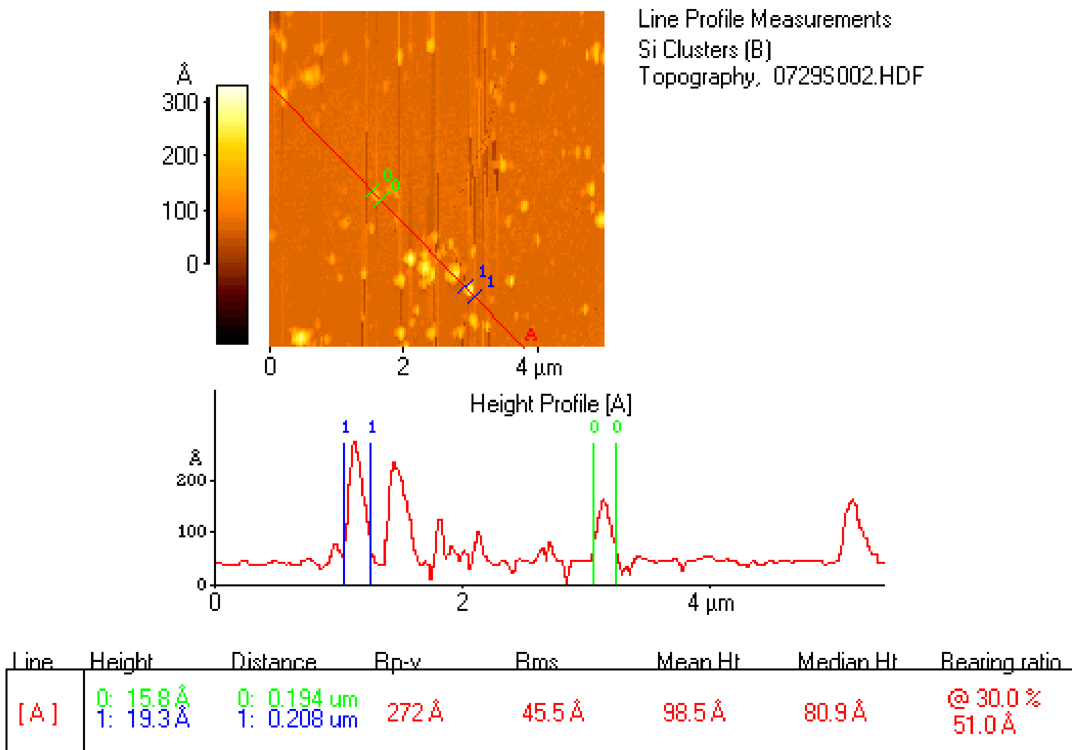

Figure 4 a) Atomic force microscope image of silicon nano-clusters on HOPG.

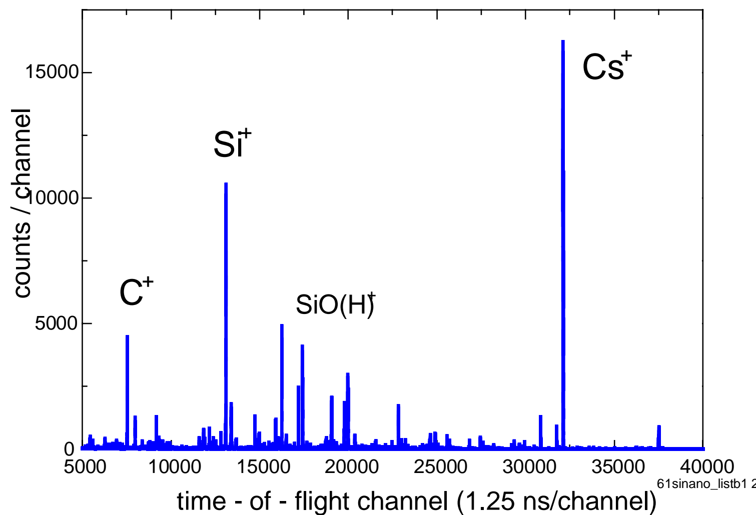

Figure 4 b): Section of a TOF spectrum of secondary ions from the cesiated Si-cluster sample.

3.2. Secondary cluster ions and coincidence analysis

In a second example the targets were SiO_2 wafers which had been coated with $CuSO_4$ [13, 25]. The surface coverage of the copper oxide was ~0.01 monolayers. Fig. 5 a) shows correlation coefficients with very strong correlations between copper and copper oxide molecular ions. These correlations indicate the presence of well separated copper oxide and silicon dioxide areas on the surface and would not be expected for a blanket deposit of evenly separated copper oxide molecules. The latter is energetically unfavorable and the formation of islands has been studied extensively in the context of the early stages of thin film growth. Fig. 5 b) shows a section of an HCI-SIMS spectrum with positive secondary ions emitted from the $CuSO_4/SiO_2$ sample.

The detection of copper oxide clusters is consistent with the presence of copper oxide islands or particles on the surface. It is an important question whether the copper contamination on SiO_2/Si surfaces is present as isolated copper molecules which can diffuse into the silicon and possibly poison the junction of a device, or if the copper is bound at the surface. The detection of cluster large copper clusters and results from the coincidence analysis both show the presence of copper particles rather than isolated molecules. This example demonstrated how coincidence analysis gives insight into the chemical structure and elemental composition of nanometer scale particles on surfaces. The information on the nano-environment of a selected species is delivered with an effective spatial resolution of about 10 nm, a regime where chemical analysis by conventional TOF-SIMS is very challenging.

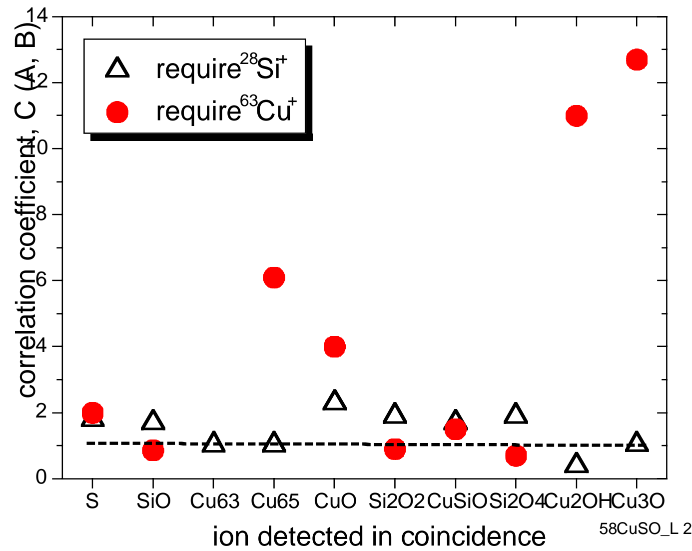

Figure 5 b) Correlation coefficient for copper and silicon secondary ions from a SiO_2/Si target with a coverage of ~1% of a monolayer of $CuSO_4$. Projectiles were Xe^{48+} at E_{kin}=557 keV.

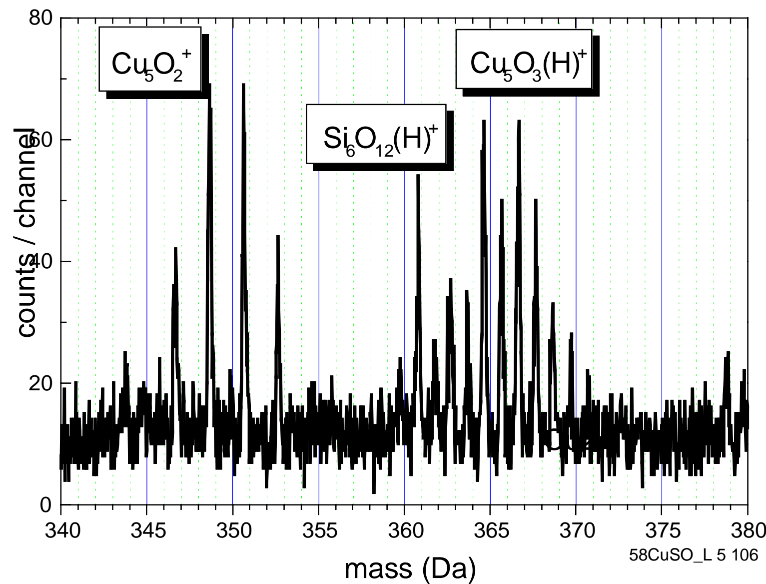

Figure 5 b): Sections of TOF-SIMS spectra from SiO_2 areas between Cu-SiO_2 structures within a die post CMP rinsed with de-ionized water.

3.3. Influence of the kinetic energy of projectiles

Sputtering and secondary ion emission in the interaction of SHCI with solids are dominated by the deposition of potential energy. Contrary to collisional sputtering with

singly charged ions, the impact energy of projectiles and the deposition of kinetic energy through electronic (inelastic) and nuclear (elastic) energy loss processes have only a minor influence [11, 16].

The projectile energy can be varied by selecting an extraction voltage from the ion source at a given retarding target voltage. The impact energy of projectiles is given by

$$E_{kin} = q \cdot (U_{extr} - U_{sample})$$

Where U_{extr} is the extraction potential, U_{sample} is the sample bias and q is the charge state of projectiles. In Figure 6, we show the ratio of positive carbon to silicon secondary ions as a function of kinetic energy of SHCI. For energies below 10 keV, the ration increases, i. e., more carbon and fewer silicon ions are emitted. The samples was a SiO_2 film on silicon that showed significant hydrocarbon contamination of unknown thickness. The low impact energy corresponds to a velocity of about 8.4×10^4 m/s, and highly charged ions travel only about 0.6 nm during a relaxation time of 7 fs. This finding is consistent with the increasing density of electronic excitation when SHCI equilibrate and deposit their potential energy in the top two or three monolayers of a material, a depth comparable with the depth of origin of secondary ions. Secondary ion emission is a consequence of the deposition of potential energy, increasing the impact energy from 30 keV to 150 keV leaves secondary ion yields [11] and the C^+ to Si^+ ratio constant.

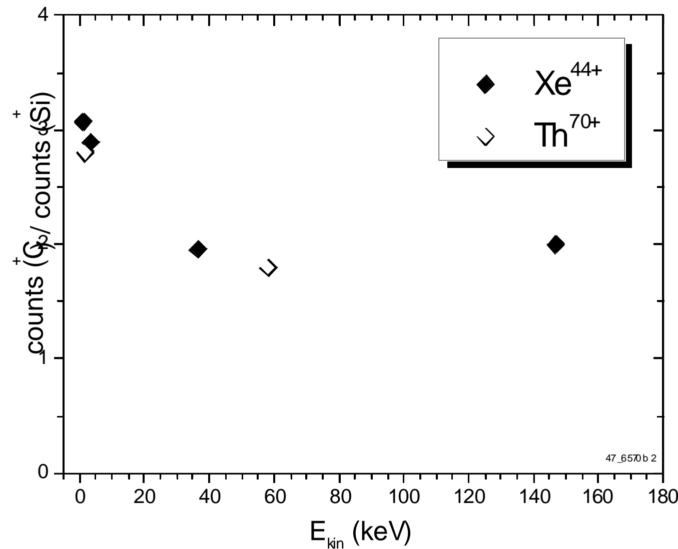

Figure 6: Ratio of carbon and silicon positive secondary ion counts from a hydrocarbon covered SiO_2/Si samples as a function of the kinetic energy of Xe^{44+} and Th^{70+} projectiles.

3.3 Ion Emission Microscope

The intense, localized and ultrafast electronic excitation of a surface by the equilibration of a slow, highly charged ion results in high yields of secondary electrons, positive and negative secondary ions as well as molecular ions. These high yields are used to image surfaces in the highly charged ion based emission microscope that was developed at Lawrence Livermore National Laboratory and is now located at Lawrence Berkeley National Laboratory [14]. SHCI are extracted from EBIT and impinge as an

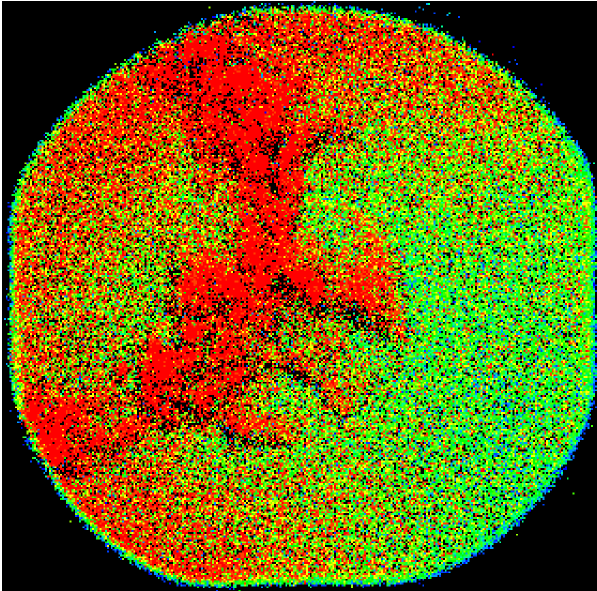

Figure 7 a): Image of a scratch on a glass lens based on secondary electron emission contrast. The field of view is 1 mm, the magnification was 40x. Charge compensation was achieved with a pulsed, low energy electron gun. Projectiles were Xe^{48+} at 700 keV.

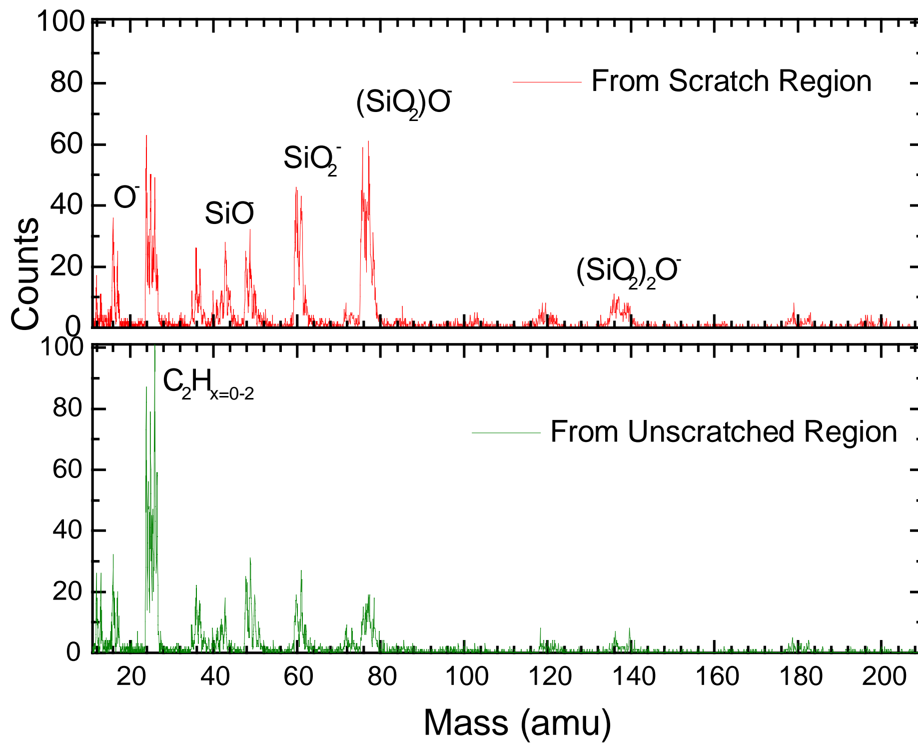

Figure 7 b): Negative secondary ion spectra collected from a scratched (top) and unscratched (bottom) region of the lens.

unfocused flood beam on a sample. An objective (immersion) lens accelerates the particles emitted at the surface, which in this case are either secondary electrons (like IEEM, ion emission microscopy [26]) or H^+ ions through the flight tube to a position

sensitive micro channelplate detector (PSD). The flight time between start pulses from electrons (in negative polarity) or protons (in positive polarity) and stop pulses from trailing secondary ions is used to determine the mass-to-charge ratio of the secondary ions. Secondary electron yields of a few hundred have been observed using HCI-SIMS. For positive-mode HCI-SIMS, the yield for protons is ~10 for Xe^{44+}. The first prototype instrument has demonstrated a resolution of 800 nm in the imaging of copper lines on silicon based on secondary electron contrast [14]. In positive polarity, a resolution of 2 μm was achieved. Investigations of resolution limiting factors such as the energy spread of secondary electrons and ions are in progress.

In Fig. 7 a) we show an example of a relatively low resolution image of a scratch on a quartz lens with 700 keV Xe^{48+} ions. Contrast is based on secondary electron emission. Charge compensation was achieved with a pulsed low energy electron gun. Spectra of negative secondary ions collected in parallel with the electron pulse height image are shown in Fig. 7 b). The spectrum on the left shows secondary ions emitted from the scratched region. The spectrum from the unscratched region (right) exhibits large peaks of surface contaminants. An important and challenging problem that is being addressed with HCI emission microscopy is that of damage mechanisms in optical components exposed to high power laser pulses. Here, the integration of coincidence analysis with emission microscopy at improved resolution holds the promise to enable significant advances.

4. Conclusion

The characteristics of secondary ion emission induced by slow (<10 keV/u), highly charged ions, like Xe^{44+}, make these exotic projectiles interesting candidates for the development of a surface analysis tool that can address challenges for particle analysis critical for sub 100 nm semiconductor technology nodes. High ionization probabilities for positive secondary ions and high yields of molecular ions enable the sensitive analysis of nano-clusters on surfaces. Current EBIT technology allows the extraction of about 1E6 Xe^{44+} ions/s, but currently available EBIT systems were not optimized for ion extraction. Recent calculations have identified venues to increase both the beam current and brightness [27]. The recently achieved ~1E4 ions/s in a 5 micron spot must be viewed as a first step in an ambitious beam focusing program at LBNL. The latter is also motivated by the development of a single ion implantation system for the fabrication of qubit arrays of ^{31}P ions for solid state quantum computer development [28]. HCI-SIMS with coincidence analysis only needs 10^3 Xe^{44+} ions/s in a spot of ~100 nm to address critical analysis issues. An ideal system would combine an SEM for particle localization with a focused highly charged ion beam for the extraction of a maximal amount of information on elemental composition and chemical structure from nano-particles on semiconductor surfaces.

Acknowledgements

This work was supported by the U. S. Department of Energy under Contract No. DE-AC03-76SF00098 and in part by the National Security Agency (NSA) and Advanced Research and Development Activity (ARDA) under Army Research Office (ARO) contract number MOD707501. Work at LLNL was performed under the auspices of the U. S. Department of Energy by Lawrence Livermore National Laboratory under contract

No. W-7405-ENG-48. A. K. was supported by the Deutsche Akademische Austauschdienst (DAAD).

References:

[1] ITRS, http://public.itrs.net/files/1999_SIA_Roadmap/Home.htm
[2] C. B. Murray, C. R. Kagan, M. G. Bawendi, Ann. Rev. Mat. Sc. 30, 545 (2000)
[3] Y. Uritsky, L. Chen, S. Zhang, S. Wilson, A. Mak, C. R. Brundle, J. Vac. Sc. Technol. A 15, 1319 (1997)
[4] R. Levi-Stetti, Y. L. Yang, and G. Gcrow, J. Phys. (Pais), Colloq. 45, 179 (1984)
[5] F. A. Stevie et al., J. Vac. Sci. Technol. B 17, 2476, (1999)
[6] R. Hull, J. Demarest, D. Dunn, E. A. Stach, and Q. Yang, Microsc. Microanal. 4, 308 (1998)
[7] B. Tomiyasa, I. Fukuju, H. Komatsubara, M. Owari, and Y. Nihei, Nucl. Instr. and Meth. B 136, 1028 (1998)
[8] D. Verkleij, Microelectronics Reliability 38, 869 (1998)
[9] A. C. Diebold et al., J. Vac. Sci. Technol. B 16, 3148, (1998)
[10] E. R. Fuoco, G. Gillen, M. B. J. Wijesundra, W. E. Wallace, and L. Hanely, J. Phys. Chem. B 105, 3950 (2001)
[11] T. Schenkel et al., Nucl. Instr. and Meth. B 161, 65 (2000)
[12] A. V. Hamza et al., J. Vac. Sci. Technol. A 17, 303 (1999)
[13] T. Schenkel, K. J. Wu, H. Li, M. W. Newman, A. V. Barnes, and A. V. Hamza, J. Vac. Sci. Technol. B 17, 2331 (1999)
[14] A. V. Hamza, A. V. Barnes, E. Magee, M. Newman, T. Schenkel, J. W. McDonald, and D. H. Schneider, Rev. Sci. Instr. 71, 2077 (2000)
[15] M. Hattass, et al., Phys. Rev. Lett. 82, 4795 (1999); T. Schenkel, et al, Phys. Rev. Lett. 79, 2030 (1997)
[16] T. Schenkel, et al., Phys. Rev. Lett. 80, 4325 (1998)
[17] K. Wien, Rad. Eff. Def. Solids 109, 137 (1989); R. E. Johnson, and B. U. R. Sundqvist, Physics Today, March 1992, P. 28
[18] R. E. Marrs, P. Beiersdorfer, D. Schneider, Physics Today, V47, 27, (1994), and references therein
[19] T. Schenkel, et al., *Phys. Rev. Lett.* 78, 2481 (1997)
[20] J. Burgdörfer, and Y. Yamazaki, Phys. Rev. A 54, 4140 (1996)
[21] T. Schenkel, et al., Phys. Scripta T80, 73 (1999)
[22] R. E. Marrs, D. H. Schneider, and J. W. McDonald, Rev. Sci. Instr. 69, 204 (1998)
[23] T. Schenkel et al., J. Vac. Sci. Technol. B 16, 3298 (1998)
[24] D. Schneider, et al., Surf. Sci. 294, 403 (1993)
[25] T. Schenkel, et al. Nucl. Instr. and Methods in Phys. Research B 161-163, 65 (2000)
[26] B. L. Doyle, et al., Nucl. Instr. and Methods in Phys. Research B 158, 6 (1999)
[27] R. E. Marrs, Nucl. Instr. and Methods in Phys. Research B 149, 182 (1999)
[28] T. Schenkel, to be published